Historical variability in Atlantic meridional baroclinic transport at 26.5°N from boundary dynamic height observations

Hannah R. Longworth [a], Harry L. Bryden [a,*], Molly O. Baringer [b]

[a] School of Ocean and Earth Science, University of Southampton, Empress Dock, Southampton, SO14 3ZH, UK
[b] NOAA Atlantic Oceanographic and Meteorological Laboratory, 4301 Rickenbacker Causeway, Miami, FL 33149, USA

ARTICLE INFO

ABSTRACT

The strength of the Atlantic Meridional Overturning Circulation (MOC) at 26.5°N may be inferred from the combination of Florida Straits transport (derived from cable measurements), Ekman transport estimated from wind stress climatologies and mid-ocean geostrophic shear (traditionally obtained from hydrographic sections) with application of mass balance to the section to yield the mid-ocean barotropic flow. The recent Rapid monitoring project has provided time series information for the mid-ocean geostrophic shear since 2004. This work presents methods to assemble a comparable dataset from CTD end stations and boundary mooring temperature and pressure time series to estimate the past variability from 1980 to 2005. Variability in the end station derived transport anomalies suggests that the MOC has fluctuated by more than 10 Sv, encompassing all MOC estimates reported in the literature. Interannual changes in MOC transport are masked by this variability and calculated trends in layer transports are not statistically significant. More extensive datasets of CTD casts and moored temperature records at the western boundary do show significant changes with warming in the thermocline and long-term freshening of the deep waters between the 1980s and 2005. These changes are associated with stronger southward flow in the upper waters and weaker southward flow in the deep waters, and suggest a decrease in the MOC strength of 2–4 Sv. Any such decrease, however, is masked by the scale of variability in layer transports derived from the historical database of CTD end stations.

© 2011 Elsevier Ltd. All rights reserved.

1. Introduction

In broad terms, the Meridional Overturning Circulation (MOC) at 26.5°N may be conceptualised as a northward flowing Florida Current through Florida Straits, northward wind driven Ekman transport in the surface layer and a net southward mid-ocean geostrophic transport. Transport estimates of each component therefore provide a method of inferring the strength of the MOC, an approach that forms the basis of studies at 26.5°N to compute circulation snapshots from transatlantic hydrographic sections (e.g. Hall and Bryden, 1982; Roemmich and Wunsch, 1985; Lavín et al., 1998, Bryden et al., 2005) and to monitor it (e.g. Hirschi et al., 2003; Cunningham et al., 2007). Monitoring the strength of the Atlantic MOC is a particularly pertinent issue, given the predicted weakening of its thermohaline component under scenarios of human induced increased atmospheric greenhouse gas concentrations (e.g. Cubasch et al., 2001) and associated cooling of western European climate (e.g. Stouffer et al., 2006).

Prior to deployment of the Rapid monitoring array (in 2004), mid-ocean geostrophic shear observations were primarily snapshots resulting from transatlantic hydrographic sections (e.g. Bryden et al.,

2005). This contrasted with the higher temporal resolution datasets available for study of the other MOC components at 26.5°N. Estimation of interannual fluctuations of both the Ekman and Florida Straits components was feasible, given wind stress climatology products extending back to at least 1980 (e.g. the NOC global monthly mean wind stress climatology, Josey et al., 2002; Berry and Kent, 2009) and a largely complete record of daily cable-derived Florida Current transports at 27°N from 1982 to the present (Baringer and Larsen, 2001). Although we are now able to study circulation changes of the mid-ocean geostrophic component on weekly timescales with the Rapid array (Cunningham et al., 2007 hereinafter CKR2007), the relatively recent deployment of the monitoring system and thus its short dataset impose limitations for assessment of interannual variability. Extension of the mid-ocean geostrophic transport time series backwards in time is therefore desirable and motivates this study. To achieve maximum consistency with the methods of the operational Rapid monitoring array and with previous analyses of hydrographic sections, this work explores the potential of using high quality oceanographic observations from 1980 to 2005 near the eastern and western boundaries of the 26.5°N section.

The "typical" MOC strength near 26.5°N defined as net northward transport above 800 m is approximately 18 Sv, with estimates ranging from 13 to 23 Sv, using simple mass balances (e.g. Bryden et al., 2005), more sophisticated inverse models (e.g. Ganachaud, 2003) and model studies (Wunsch and Heimbach, 2006). Eight hundred metres

---

corresponds to the maximum depth of the Florida Straits, through which the long-term mean northward transport is 32.2 Sv (Baringer and Larsen, 2001). The mean Ekman transport across this latitude computed from the NOC wind stress climatology between 1980 and 2005 is 3.1 Sv. Southward recirculation of the subtropical gyre in the mid-ocean above 800 m was 16–18 Sv in the 1957, 1981 and 1992 sections (Longworth, 2007), giving a net northward transport of the MOC's upper limb of 17–19 Sv. Below 800 m in the mid-ocean, the approximately 20 Sv southward flow of North Atlantic Deep Water (NADW) dominates, with roughly equal transport of the upper (UNADW, 1100–3000 m) and lower (LNADW, 3000–5000 m) components. Small northward transports of Antarctic Intermediate Water (AAIW) and Antarctic Bottom Water (AABW) of 2–4 Sv are found above and below the NADW (e.g. Hall and Bryden, 1982; Roemmich and Wunsch, 1985; Lavín et al., 2003), all comprising the MOC's lower limb.

The method of end stations has been used before, for example by Sato and Rossby (1995) to monitor changes in Gulf Stream transport based on hydrographic stations bracketing the Gulf Stream and by Curry and McCartney (2001) to monitor changes in North Atlantic gyre strength based on stations near Bermuda and in the Labrador Sea. Here we aim to monitor the full basin-scale mid-ocean circulation for which we require CTD stations very close to the western and eastern boundaries of the mid-ocean 26.5°N section near the Bahama and Canary Islands. This approach is consistent with analysis of both the traditional transatlantic hydrographic sections and the dynamic height moorings of the Rapid array and it relies on there being many more end stations in the historical database beyond the 5 transatlantic hydrographic sections in 1957, 1981, 1992, 1998 and 2004.

At the western boundary, where we expect greatest variability, there is indeed an extensive historical dataset of CTD stations that are associated with repeat deployments of the Abaco current metre array made between 1986 and 1998 (Lee et al., 1996) as part of the Subtropical Atlantic Climate Studies (STACS), Western Atlantic Thermohaline Transport Study (WATTS) and the Atlantic Climate Change Program (ACCP). The western boundary dataset adds between 25 and 35 end stations to the previously analysed 5 hydrographic sections, providing substantial information on the temporal variability in the mid-ocean geostrophic flow. At the eastern boundary where we expect less variability, we had hoped there would be many additional CTD stations associated with the Kiel-276 mooring deployments (Müller and Siedler, 1992) but most of these stations proved to be too far from the boundary for reliable estimates of the basin-wide geostrophic flow. As a result, the eastern boundary dataset only added 5 end stations to the previously analysed hydrographic sections.

Methods to assemble and process the historical datasets at 26.5°N and the observed variability in layer transports are described in Section 2. In Section 3, mooring time series are considered as end stations for western boundary variability. In discussing the end station observations (Section 4), we focus on interannual timescales to complement results from the Rapid array (Cunningham et al., 2007). Concluding remarks are in Section 5.

2. Historical CTD end stations

2.1. Analysis method

The theory underlying the end station method is that in the absence of intervening topography the zonal average of the mid-ocean meridional baroclinic geostrophic velocity profile may be estimated from a pair of deep hydrographic stations at either end of the mid-ocean section (Hall and Bryden, 1982; Marotzke et al., 1999; Lynch-Stieglitz, 2001). For two hydrographic stations, W and E at the western and eastern boundaries, respectively, of the 26.5°N section (referred subsequently as end stations) separated by distance Δx, the average geostrophic velocity profile (v) between W and E at pressure (p) relative to a reference pressure ($p=p_R$) with reference velocity ($v=v_R$), is given by

$$(v-v_R) = \frac{10}{f\Delta x}(\Delta D_E - \Delta D_W) \qquad (1)$$

where

$$\Delta D = \int_{p_R}^{p} \delta \, dp$$

f is the Coriolis parameter and ΔD the dynamic height relative to pressure p_R (in dbar) with specific volume anomaly δ in cm^3 g^{-1} (e.g. Pond and Pickard, 1983). Eq. (1) therefore provides a method of estimating the zonally averaged meridional baroclinic transport profile at 26.5°N under the assumption that a uniform reference level across the section is a workable simplification.

We develop Eq. (1) to allow consideration of the contribution made independently by each boundary to variability of mid-ocean baroclinic transport of water mass layers. This approach is particularly illuminating where data availability is not evenly distributed between the two boundaries. The contribution of the western (eastern) boundary is determined following Eq. (1), but with the added assumption that the density structure at the eastern (western) boundary remains unchanged. We calculate the resulting transports as anomalies relative to a pre-determined reference state. Formally, consider two end station pairs such that W_r and E_r provide an estimate of the meridional transports at an arbitrary reference time t_r and W_1 and E_1 provide an estimate at time t_1, with velocities v_r and v_1, respectively. It is easily shown from (1) that the change in the eastern (western) boundary transport per unit depth profile referenced to p_R, at time t_1 relative to t_r, assuming that western (eastern) boundary conditions remaining constant is given by

$$\Delta x(v_{E(W)_1} - v_{E(W)_R}) - \Delta x(v_{E(W)_r} - v_{E(W)_R}) = \Delta x(v_{E(W)_1} - v_{E(W)_r})$$
$$= 10(\pm\Delta D_{E(W)_1} - \pm\Delta D_{E(W)_r})/f \qquad (2)$$

The final step is to integrate the transport per unit depth anomaly profile from Eq. (2) over specified depth ranges to give the layer transport anomalies. Layers are defined to represent water masses consistent with CKR2007: the upper layer of 0–800 m corresponds to recirculating thermocline waters; the intermediate layer is 800–1100 m while the components of NADW occupy depths of 1100–3000 m (UNADW) and 3000–5000 m (LNADW) at the east or west, respectively. No attempt is made to monitor Antarctic Bottom Water (AABW) transport anomalies since it is banked up against the Mid Atlantic Ridge at this latitude (Bryden et al., 1996) and therefore is not amenable to measurement by boundary end stations.

In summary, the end station method yields a set of transport anomalies for each of the upper, intermediate and both NADW layers at either the eastern or the western boundaries computed from historical hydrographic end stations relative to a reference state. No significance is attached to the reference state since the interest of this study is in the calculation of baroclinic transport variability.

2.2. Choosing the end stations

We define the limits of the eastern and western boundary regions (Fig. 1) based on the consideration of the hydrography and circulation of the region (full details in Longworth, 2007). The primary consideration in selecting end-point stations is to find
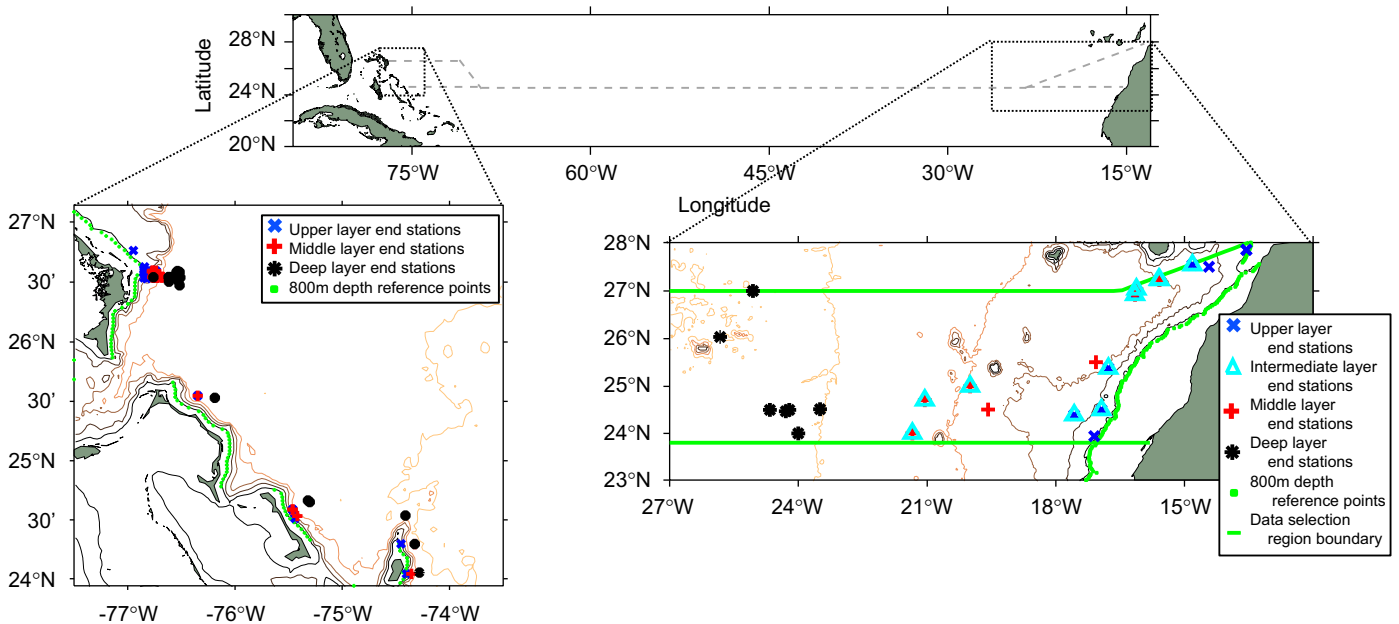
Fig. 1. Locations of the eastern and western boundary study regions in relation to the cruise tracks of the 24.5°N transatlantic sections shown with dashed lines of the upper plot (e.g. Bryden et al., 2005). Selected end stations shown in each boundary region along with the 800 m isobath. At the west, no stations are taken west of San Salvador Spur (74.5°W, 24°N) due to intervening topography. Depth contours are indicated at 1000 m intervals to 5000 m with land shaded.

Table 1
Layer transport anomalies (Δtr) at the eastern boundary. N is the number of observations, μ and σ the mean and standard deviation of Δt_r for the given layer, respectively. The overall estimated error in Δt_r (total) of each layer is the r.m.s. combination of the observational error (Obs: the r.m.s. combined estimated error due to pressure, salinity calibration and temperature uncertainties) and location error (that due to end station offshore position). Last 3 columns refer to linear regression to $\Delta tr = A$ (year after 1980) + B with 95% confidence interval given for A. R^2 is the percent of variance of each time series explained by the regression, and the final column the transport change over 25 years according to the fitted trend (as plotted in Fig. 3).

	N	μ (Sv)	σ (Sv)	Range (Sv)	Error in Δt_r (Sv)			A ($\times 10^{-4}$ Sv day^{-1})	R^2 (%)	25 yr Δt_r
					Obs.	Location	Total			
0–800 m	10	−0.6	2.0	6.9	0.7	1.0	1.2	−1.37 ± 6.0	3	−1.2
800–1100 m	11	0.2	0.5	1.7	0.3	1.0	1.0	0.55 ± 1.4	13	0.6
1100–3000 m	9	0.1	1.6	5.0	1.6	2.0	2.6	0.82 ± 3.0	6	0.7
3000–5000 m	7	0.0	0.6	1.3	1.0	1.0	1.4	−0.27 ± 1.6	1	−0.1

reasonable quality data close enough to the boundary so that no appreciable transport would be "lost" between the station and the boundary. Each layer is treated separately and a good CTD cast must include data throughout the entire layer in question. Except for the 1957 24°N section, we found no stations close to the eastern or western boundary prior to 1981. Thus, we consider the time period from 1981 to 2005, excluding the 1957 stations because their values 24 years before any other observations completely determined the size of any trends with time.

In order to estimate reasonably acceptable distances from the eastern boundary, the 25°N transatlantic hydrographic sections were used to estimate how far westward one could go before the accumulated transport exceeded 1 or 2 Sv. The resulting distances are water mass dependent with 160, 500, 500 and 1000 km offshore distances for each of the upper, intermediate, middle and deep layers, respectively. CTD casts separated by at least 2 days in time are obtained from the World Ocean Database 2001, Hydrobase, WOCE, NOC and IFM-Kiel datasets for each layer, rejecting any sample which is in a meddy. The result is a set of 10, 11, 9 and 7 end stations for each transport anomaly layer (Fig. 1, Appendix 1), which are judged representative of 26.5°N eastern boundary conditions. The relatively small dataset of CTD casts for eastern boundary end stations is not ideal for resolution of interannual variability of meridional baroclinic transports

originating at this boundary but it is the best we could find in the historical database.

At the western boundary, consideration of accumulated transports from the transatlantic hydrographic sections (Bryden et al., 2005) and boundary hydrographic sections (Leaman and Harris, 1990) led us to define offshore limits for end stations of 14, 20, 20 and 37 km for each of the upper, intermediate, middle and deep layers, respectively (Longworth, 2007). CTD stations separated by at least 1° in latitude and 7 days in time are extracted for each of the study layers from the World Ocean Database, Hydrobase and NOAA/AOML archives resulting in 39 stations for each of the upper and intermediate/middle layers and 29 stations for the deep layer (Fig. 1, Appendix 2).

For each layer transport at each boundary, we assign a location error (Tables 1 and 2) based on the accumulated transports found in the transatlantic hydrographic sections out to the offshore boundary chosen for each layer.

2.3. Processing the CTD stations

While careful data selection minimises the transport anomaly error due to station location (Table 1), possible errors associated with data accuracy remain. At the eastern boundary, the selected

Table 2
Layer transport anomalies (Δt_r) at the western boundary. N is the number of observations, μ and σ the mean and standard deviation of Δt_r for the given layer, respectively. All column definitions are as in Table 1, and linear regression parameters refer to those plotted in Fig. 6.

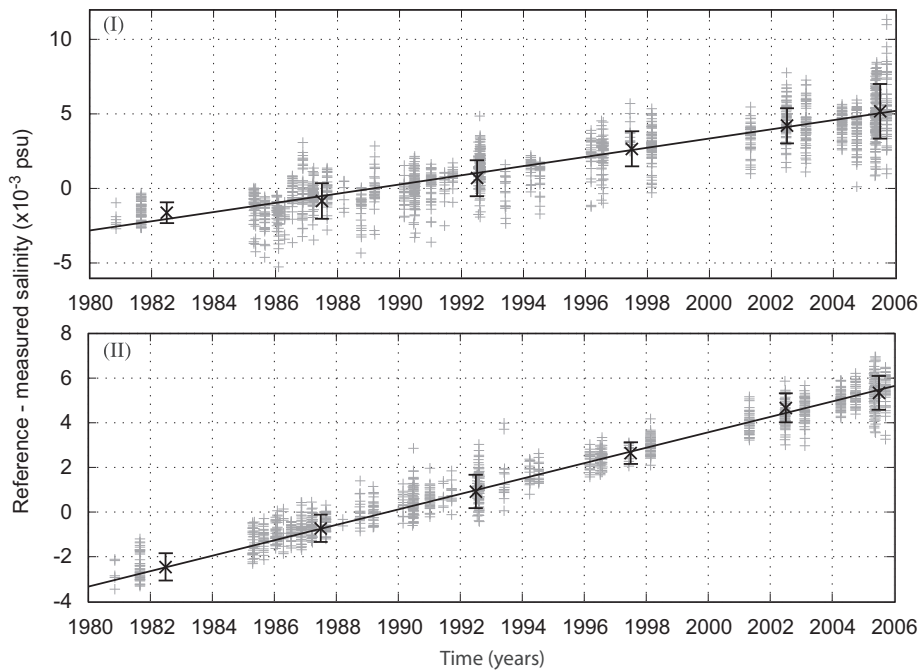|	N	μ (Sv)	σ (Sv)	Range (Sv)	Error in Δt_r (Sv)			A ($\times 10^{-4}$ Sv day^{-1})	R^2 (%)	25 yr Δt_r
					Obs.	Location	Total			
0–800 m	39	0.6	2.8	10.4	0.3	2.0	2.0	-0.52 ± 3.6	0.2	-0.5
800–1100 m	39	0.0	0.1	0.6	0.1	0.2	0.2	0.04 ± 0.2	0.6	0.0
1100–3000 m	39	0.0	2.5	10.8	1.3	2.0	2.4	1.41 ± 3.3	2.0	1.3
3000–5000 m	29	0.7	4.2	17.3	2.8	3.0	4.2	2.64 ± 6.4	2.6	2.4

Fig. 2. Salinity anomalies (Hésperides reference minus measured) on 0.1 °C potential temperature levels between 2.55 and 2.95 °C for ISOW (I), and 1.95 and 2.45 °C for DSOW (II) as a function of time. CTD casts are within 150 km of the 800 m isobath between 24 and 27°N. Linear regression over time of the 5-year mean salinity anomalies from 1980 to 2005 and 2005–2006 annual mean ($\times$) (with error bars of $\pm 2\sigma$) after rejection of points outside the mean ± 0.003 (--) shows freshening over the 25 years at approximately 0.0031 and 0.0034 per decade for ISOW and DSOW respectively.

CTD casts' salinity range of 0.008 on potential temperature surfaces in the deep water is in sharp contrast with Saunders' (1986) constant potential temperature–salinity (θ–S) relationship in this region over 2.0–2.5 °C. While Mantyla's (1994) review of this relationship found a latitudinal dependence, it is negligible amounting to a salinity change of only 0.0002 at 2.0 °C between 23.8°N and 28°N. Thus we argue that the deep salinity variability in our raw dataset is due to measurement errors and hence CTD casts are calibrated by addition of an offset such that the mean offset relative to a reference station from the 1992 Hésperides transatlantic section is zero over the deepest 0.1 °C potential temperature levels between 2.05 and 2.45 °C. Of the 26 distinct end stations, 16 are deep enough to be calibrated (Appendix 1).

At the western boundary, the selected end stations have a salinity range of approximately 0.01 on potential temperature levels in deep water. In contrast to the eastern boundary variability, we believe this is at least partly due to a freshening over time of LNADW consistent with the overflow freshening signal (Dickson et al., 2002) reaching the subtropics. Salinity anomalies of the Denmark Straits Overflow Water (DSOW, 1.9–2.5 °C) and Iceland Scotland Overflow Water (ISOW)/North Atlantic Interior Waters (NAIW) mixture found between 2.5 and 3.2 °C (Fine and Molinari, 1988; Fine, 1995; Molinari et al., 1998) on 0.1°C potential temperature surfaces from 280 CTD casts within

150 km of the 800 m isobath relative to a 1992 Hésperides reference station show dramatic freshening over time (Fig. 2). Linear regression of 5-year mean salinity anomalies for each layer is significant at 99% confidence level and amounts to freshening of 0.0085 and 0.0077 from 1980 to 2005 for DSOW and ISOW, respectively. Standard deviations of each 5-year mean are less than 0.001 for DSOW and 0.002 for ISOW, both smaller than the anticipated salinity measurement error in the western boundary of 0.003 (Vaughan and Molinari 1997). Thus the trend over the 25 years is judged to be significant so selected end stations that resolve DSOW are calibrated by applying an offset such that the resulting mean difference between the calibrated salinity and a time varying reference derived from the linear regression of salinity anomaly with time plotted in Fig. 2(II) on 0.1°C potential temperature levels of DSOW is zero (or of ISOW for shallower casts). CTD casts shallower than ISOW are not calibrated since Labrador Sea Water (LSW) θ–S changes are better described by oscillations over the considered timeframe (Vaughan and Molinari, 1997). Of the 92 CTD casts selected as end stations, 65 are calibrated based on the DSOW region of the θ–S curve and 3 based on ISOW (Appendix 2).

Transport anomalies in the east are computed following Eq. (2) relative to a reference dynamic height profile, which itself is obtained from the mean specific volume anomaly of the selected

end stations in the layers. Dynamic heights are referenced to 3200 dbar, consistent with previous transport calculations at this latitude (Saunders, 1987; Arhan et al., 1994; Lavín et al., 1998). In the west, transport anomalies are computed similarly following Eq. (2), relative to a reference profile computed separately for each layer as the mean of the calibrated CTD casts selected as end stations. Dynamic height anomaly profiles are referenced to 1000 dbar, consistent with geostrophic transport calculations in the region (Olson et al., 1984; Leaman and Harris, 1990).

Errors in transport anomalies are assessed by calculation of the change in transport anomaly resulting from separate additions to all end stations of a uniform salinity offset, ΔS of 0.005, a temperature offset, ΔT, of 0.002 and a pressure offset, Δp, of 3.5 dbar. The root mean square (r.m.s.) transport anomaly errors due to each of these additions are combined also in an r.m.s. sense to give the "observation error" of Tables 1 and 2. The combined observation and location errors associated with each layer transport anomaly are then estimated. In the east the overall error is less than ± 1.5 Sv for all layers except that of UNADW for which it is ± 2.6 Sv (Table 1). In the west, the overall uncertainty is ± 2, ± 0.2, ± 2 and ± 4.2 Sv for the upper, intermediate, middle and deep layers, respectively (Table 2) and is dominated by the "location" component, that is by the possible transport inshore of the end station.

2.4. Eastern boundary layer transport variability

Fig. 3 shows the layer transport anomalies for all eastern boundary end stations added to mid-ocean geostrophic layer transports computed from the 1992 Hésperides transatlantic hydrographic section. The end station transport anomalies are representative of the variability originating at the eastern boundary around a possible long term mean. Linear least squares regression trends of all layer transport anomalies with time (Fig. 3 and Table 1) are not significant and the lower water column anomalies (intermediate, middle and deep layers) are negligible in magnitude, amounting to transport changes of less than 1 Sv between 1980 and 2005 and smaller than each layer's respective error estimate. Also the observed range in transport anomalies for the lower layers is encompassed by the total estimated error (Table 1). Thus, the variability observed in the intermediate, middle and deep layer transport anomalies at the eastern boundary is small and indistinguishable from noise. On the other hand, upper layer transport anomalies at the east do

show a range significant above the estimated error (6.9 Sv range versus 1.2 Sv error, Table 1). Linear regression shows a trend towards increasingly negative transport anomalies over time, indicative of a 1.2 Sv increase in southward geostrophic transport of the thermocline waters between 1980 and 2005 (Fig. 3, Table 1). The trend is not significant at the 95% level (Table 1), which is not surprising given that its magnitude is comparable to the method error of 1.2 Sv (Table 1).

Whether or not there is a seasonal dependence in the upper transport anomalies at the east is difficult to ascertain because there are only 10 data points spread over 8 months of the year, potentially contaminating any estimate of interannual variability. A seasonal cycle in the upper layer transport anomalies might be hypothesised based on the annual upwelling cycle. Between 20°N and 25°N upwelling is fairly strong and steady year round, but between 25°N and 28°N (the north of our study region) upwelling is weaker overall and particularly in winter/spring (Mittelstaedt, 1991). Although upwelling is strictly confined to a narrow strip of shelf waters 20–30 km from the coast, the effects may also be felt over the shelf break, where we ideally select upper layer end stations. In an upwelling scenario, winter/spring end stations north of 25°N would be expected to have warmer thermoclines (relative to the strong upwelling case), which as illustrated in Fig. 4, decreases the basin-wide thermocline slope (assuming no change at the west) and leads to weaker southward transport across the mid-ocean. This is expressed in end station calculations as a positive upper layer transport anomaly at the east. The three most positive upper layer transport anomalies (2.1, 0.9 and 1.2 Sv) do occur in winter/spring end stations north of 25°N (grey circles of Fig. 5(I) including November 1984), consistent with the seasonal upwelling influence hypothesis, and can be seen in the stations' high 400 m temperatures (Fig. 5(II)). The May 2004 upper layer transport anomaly is −2.6 Sv suggesting that individual events (in addition to a possible seasonal cycle) cannot be ignored. We conclude that there may well be a seasonal dependence in the transport anomalies of six upper layer end stations north of 25°N, resulting in seasonal extremes of the order ± 1 Sv (Appendix 1), but the data is insufficient to resolve and justify its removal.

2.5. Western boundary layer transport variability

Fig. 6 illustrates variability in the mid-ocean baroclinic layer transports originating at the western boundary of 26.5°N between
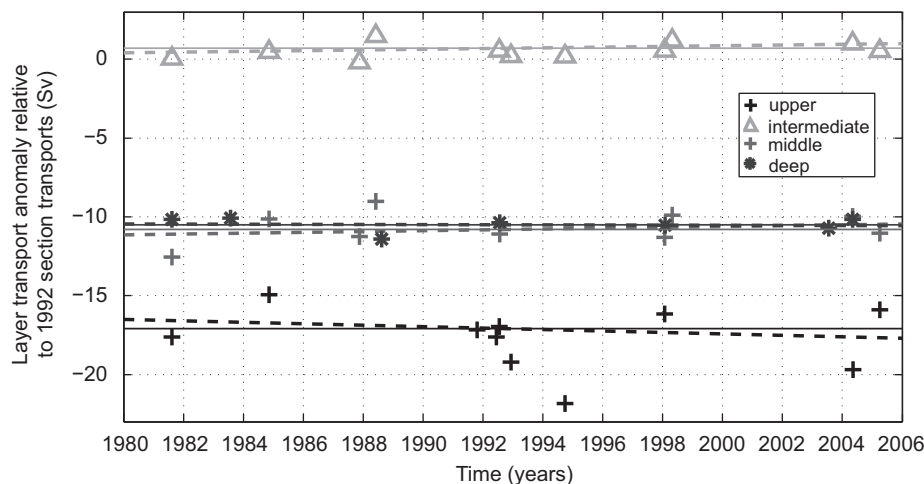
Fig. 3. Transport variability of the upper (+, 0–800 m), intermediate (△, 800–1100 m), middle (+, 1100–3000 m), and deep (✳, 3000–5000 m) layers originating at the eastern boundary. Data points plotted are the end station layer transport anomalies added to typical layer transports across the mid-ocean of −17.1, 0.7, −10.8 and −10.5 Sv, respectively (computed from the 1992 Hésperides transatlantic section). Thin solid lines show the reference layer transport, while the thick dashed lines are the least squares linear regressions to the transport anomalies (coefficients in Table 1).
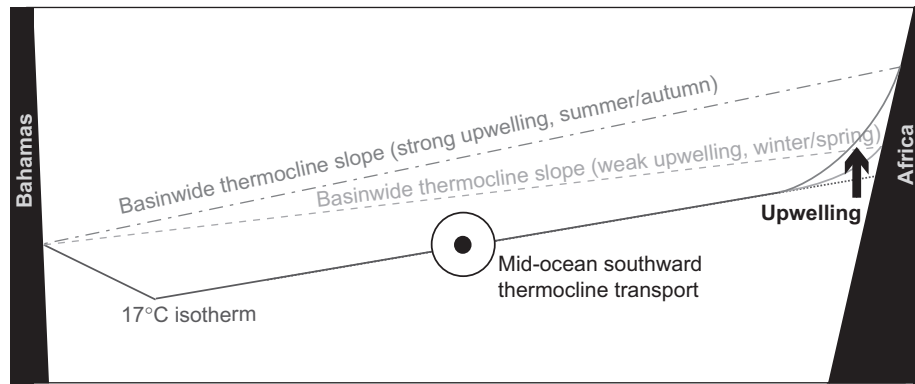
Fig. 4. Schematic of the effect of a seasonal cycle in upwelling at the eastern boundary north of 25°N on the basin-wide thermocline slope, and thus net southward transport of thermocline waters in the mid-ocean as estimated from end stations at each boundary. Only the upper water column is represented.
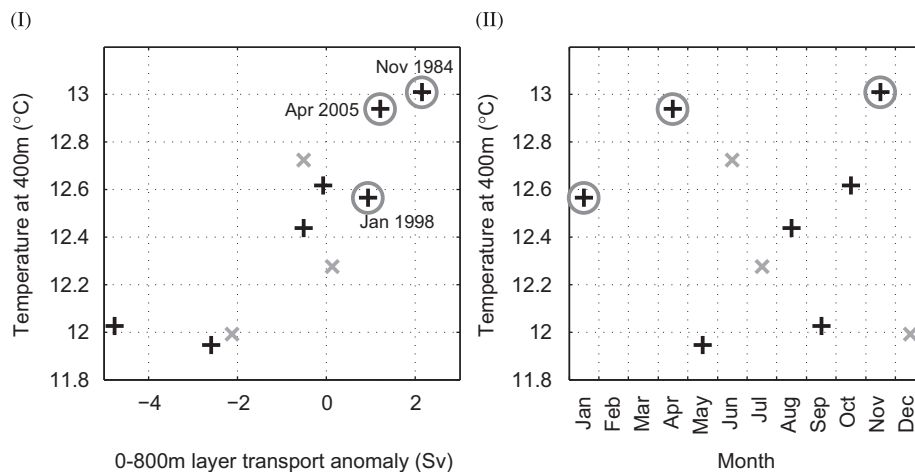
Fig. 5. (I) Correlation between eastern boundary upper layer end station transport anomalies and the temperature at 400 m. (II) Temperature at 400 m plotted as a function of month for eastern boundary end stations. In both, stations north of 25°N are plotted with (+), those south with (×) and those of November 1984, January 1998 and April 2005 circled.

1980 and 2005 derived from careful selection of high quality hydrographic stations with quantified errors (Table 2). Individual transport anomalies are plotted along with their linear regression over time (regression coefficients are in Table 2). Two- and five-year mean anomalies with error bars spanning ± one standard deviation of the constituent observations are also shown. It is readily apparent that variability of all layer transport anomalies (except the intermediate) at the west is much larger than at the east (Tables 1 and 2) on both annual and interannual periods (Figs. 3 and 6).

For the upper layer, end-station observations suggest increasing southward transport of the 0–800 m waters between the late 1980s and 2005. The trend in upper layer end station transport anomalies of a 0.5 Sv change between 1980 and 2005 (Table 2) is statistically not significant and is small in comparison with the variability observed within 2 and 5-year periods of the order ± 2–3 Sv (Fig. 6(I)). High frequency signals (e.g. Wunsch and Heimbach, 2006; Kanzow et al., 2007) are not resolved by the sampling but clearly contribute to variability within particular years.

Regarding possible sub-annual cycles in the computed transport anomalies, Lee et al. (1996) found seasonal cycles in the Antilles Current transport and DWBC transport. Lee et al. noted that the seasonal cycle in DWBC transport was a barotropic response to remote wind forcing and therefore would not contaminate the baroclinic transport anomalies computed here. For the upper layer Antilles Current variability, least squares

regression of end station transport anomalies as a function of month to a sinusoidal curve with periods of both 6 months and 1 year does show summer peaks in northward flow in phase with previous studies (Lee et al., 1996, Molinari et al., 1990, Baringer and Molinari, 1999), but the amplitudes are smaller than 1 Sv (Fig. 7(II)) compared with Lee et al. (1996)'s 7 Sv and the fits are not significant even at the 20% level. Furthermore, for the mooring dataset that exceeds 8 years duration (discussed below), none of the monthly mean anomalies in upper layer transport are significantly different from zero at the 95% confidence level. Overall the monthly anomalies have a range of only 2 Sv (Fig. 7(I)), hence available observations do not support the existence of any seasonal cycle in upper layer baroclinic transport anomalies near the western boundary larger than ± 1 Sv that would contaminate the variability of Fig. 6(I).

The variability of intermediate water transport originating at the western boundary is, as at the east, negligible with any trend smaller than 0.1 Sv over 25 years (Fig. 6(II), Table 2). The range of 5-year mean transport anomalies, including limits of ± one standard deviation, is less than 0.2 Sv, which is the size of the end station error for this layer. Transport anomalies of both NADW layers show trends towards decreased southward flow of the DWBC, amounting to reductions of 1.3 and 2.4 Sv in the upper and lower deep water layers, respectively, over the 25 years (Fig. 6(III) and (IV), Table 2). The trends are not statistically significant. The trends are broadly consistent with the freshening of LNADW at this boundary by 0.008 in 25 years, to which the end stations have
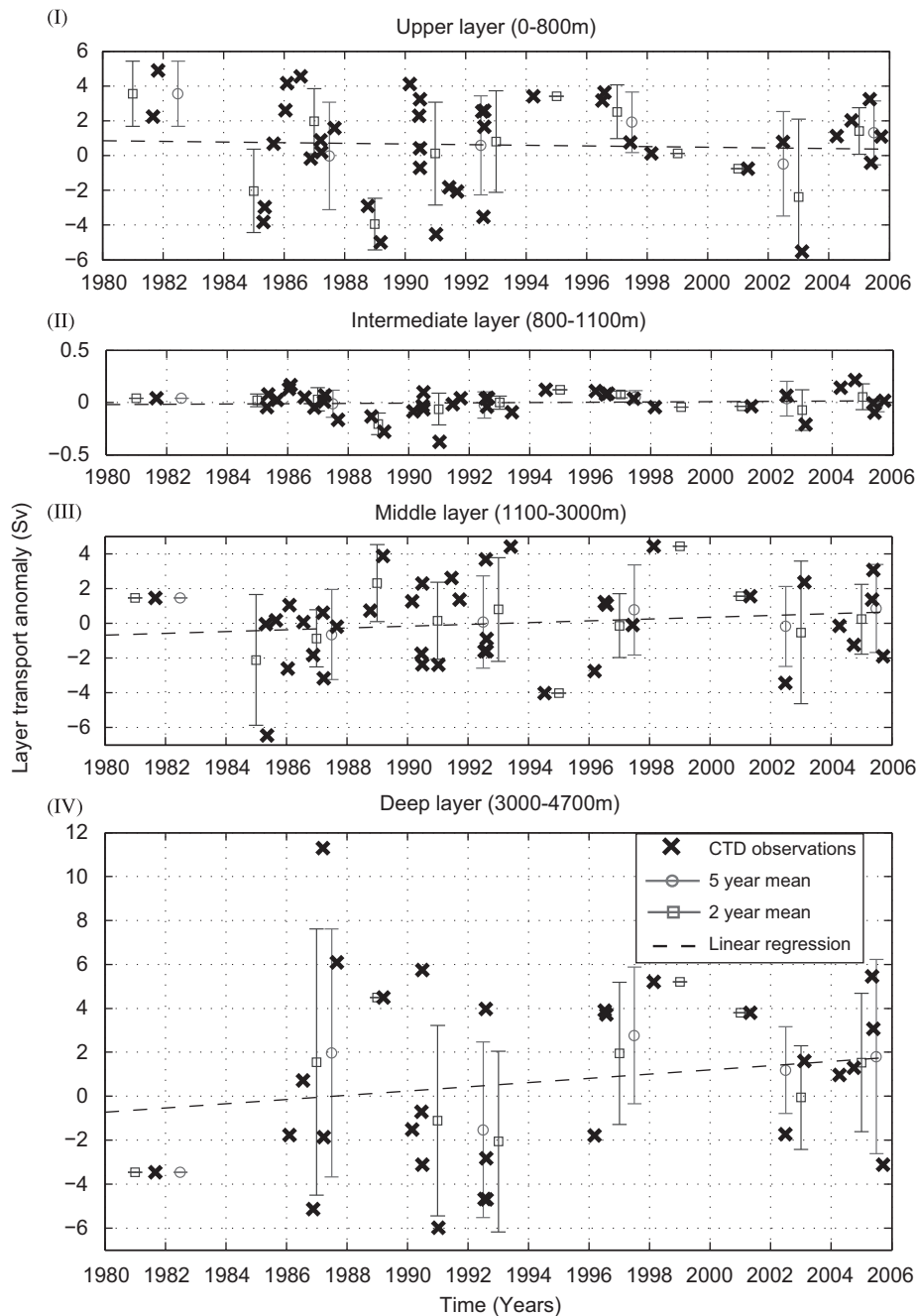
Fig. 6. Interannual variability of the upper, intermediate, middle and deep layer end station transport anomalies at the western boundary. Individual data points are plotted (×) along with their 5-year mean (○) and 2-year mean (□) with error bars of ± one standard deviation. For the 5-year means the last group is actually 2005–2006. Dashed lines are the least squares linear regression of individual data points to $\Delta tr = A$(day number after 1 st January 1980) $+ B$, where A and B (with 95% confidence intervals) for each layer are given in Table 2.

been calibrated (Section 2.3). Applying a salinity offset of -0.004 results in positive (northward) transport anomalies of 1.0 and 2.2 Sv for UNADW and LNADW, respectively. That the transport trend of 2.2 Sv in LNADW is smaller than the expected 4.4 Sv change for the observed freshening of 0.008 likely reflects unresolved high frequency variability (e.g. Wunsch and Heimbach, 2006; Kanzow et al., 2007) in addition to any possible interannual fluctuations (Fig. 6(III) and (IV)).

2.6. Summary for hydrographic end stations

All long-term trends in layer transports at the western or eastern boundary derived from the available hydrographic

dataset are not statistically significant. Calculated trends over 1980–2005 do indicate a reduction in overturning: increases in southward thermocline transport of 1.2 Sv in the east and 0.5 Sv in the west, and decreases in southward deep water transport of 0.6 Sv in the east and 1.3 Sv in UNADW and 2.4 Sv in LNADW in the west. Whilst none of these trends are statistically significant, all suggest a reduction in the MOC transport of 2–4 Sv from 1980 to 2005. Sub-annual and interannual variability in layer transports of the order 3–4 Sv masks any such trends. In the deep layers, there is a significant freshening of deep waters near the western boundary of 0.008, which should dynamically generate a reduction in southward transport of LNADW of the order 4 Sv. Even for LNADW, unresolved high frequency signals in the end
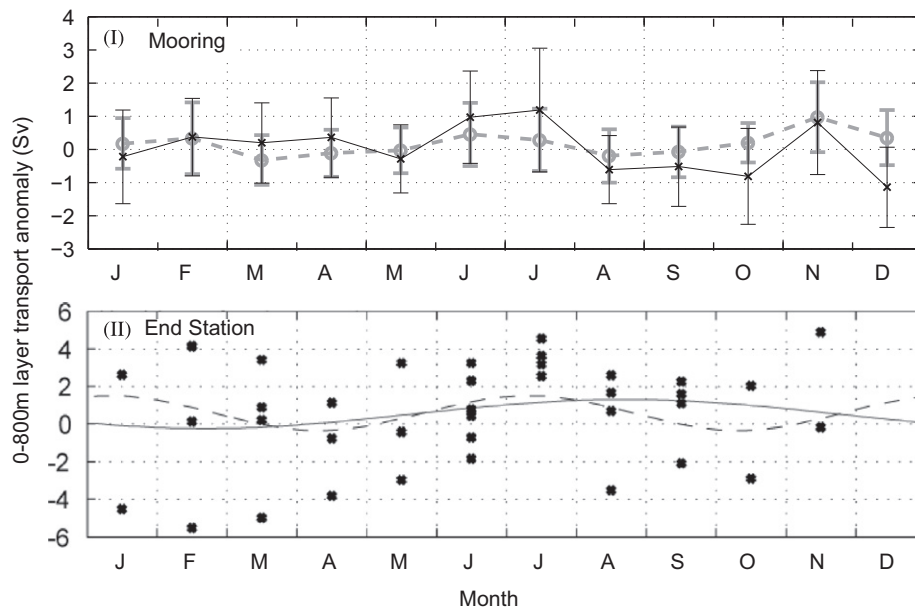
Fig. 7. Investigation of possible annual or semi-annual cycles in the western boundary upper layer transport anomalies computed from moorings (I) or end stations (II). The mooring transport anomalies are derived from either the T_{400} record – dashed line with $\circ$ or dynamic height computed from mooring temperature and pressure time series (see Longworth (2007) for details of the dynamic height calculations) – solid line with $\times$. Error bars are $\pm 2\sqrt{(\text{monthly variance}/N^*)}$ where the monthly variance is computed after removal of each period's mean and N^* is the number of independent samples per month based on integral timescales – of order 20 days for most mooring deployments (Longworth, 2007). In (II) a least squares regression of the transport anomalies as a function of month to a sinusoidal curve with variable phase shift of the form $\Delta tr_{seas} = A\cos(\omega t) + B\sin(\omega t) + C$, where $\omega = 2\pi/\tau$ and τ is either 12 months (solid line) or 6 months (dashed line), is shown.

station dataset mask any such trend towards reduced southward transport of deep water over time. Thus, despite some indications of reduced overturning, we detect no significant change in the overturning over the period 1980–2005 from our analysis of the available database of hydrographic end stations.

3. Mooring end stations

Many of the historical CTD stations near the western boundary were made during repeat deployments of the Abaco current metre array between 1986 and 1998 (Lee et al., 1996). Here we examine these mooring arrays as potential end stations. Johns et al. (2005) have derived geostrophic transports between carefully designed and instrumented mooring pairs, but in general many of the Abaco moorings are not suitable for end stations as they are located too far from the boundary. Geostrophic transports are sensitive to mooring configuration that changes between deployments, making long time series records of consistent transport difficult to construct. Here we use an alternative approach of using temperature changes at 400 dbar very close to the western boundary as nearly all of the arrays included a temperature–pressure record near 400 m depth. Used in conjunction with the set of CTD stations, we can assess the variability of upper ocean baroclinic transport from the 400 m temperature record.

Moorings A and A_1 of the Abaco array deployments are located at 26.5°N, 5 and 6 km, respectively, from the 800 m isobath and therefore lie comfortably within our western boundary study region in water depths ranging from 900 to approximately 3500 m (Appendix 3). While it is possible to obtain geostrophic transport anomalies from their temperature and pressure records through vertical interpolation and salinity estimation using climatological stratification and θ–S relationships, respectively, cross comparison between deployments is limited due to differing mooring configurations (Appendix 3), and therefore deployment dependent errors (Longworth, 2007). All deployments do however
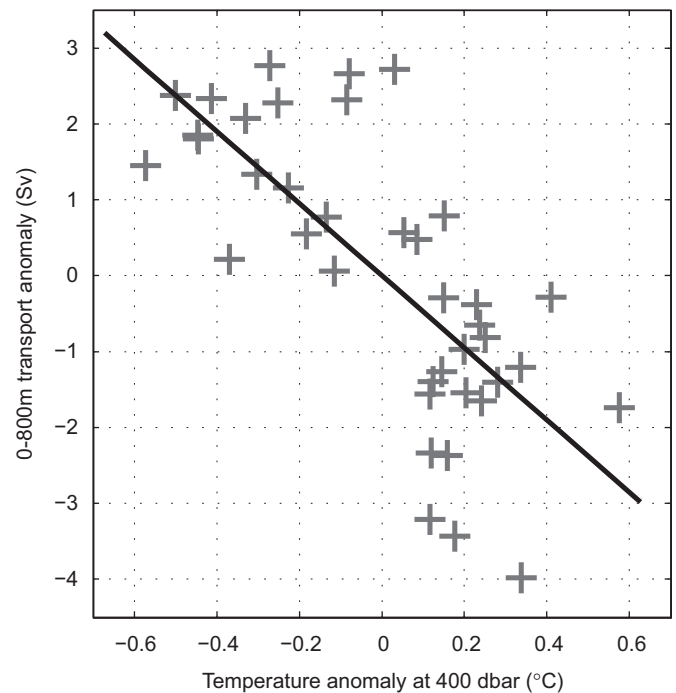
Fig. 8. Linear regression of the 0–800 m layer transport anomaly to the temperature at 400 dbar minus 17.60 °C (the group mean) for the western boundary upper layer end stations.

have temperature sensors at nominal depths within 50 of 400 m, lying conveniently at mid-depth of our upper layer. We use these to obtain a 400 dbar temperature transport anomaly proxy.

Justification for this 400 dbar temperature transport proxy comes from the strong correlation found between the transport anomaly of the 39 upper layer western boundary CTD end station

transport anomalies and their temperature anomaly at 400 dbar relative to the group mean (Fig. 8). Linear regression according to

$$\Delta Tr_{upper} = A\,(T_{400} - 17.60) + B \tag{3}$$

accounts for 53% of the variance and is significant at the 95% confidence level with $A = -4.75 \pm 1.50$ and $B = 0.00 \pm 0.42$. The r.m.s. error of the resulting transport anomaly is 1.3 Sv, which compares favourably with the estimated 2–3 Sv error in geostrophic upper layer transport anomalies using CTD end stations.

To obtain the 400 dbar temperature time series, pressures are estimated (if not measured directly) for the temperature record with nominal depth closest to 400 m using the pendulum model (e.g. Johns et al., 2005). The measured temperature at this pressure (T_p) is then corrected to 400 dbar (T_{400}) following

$$T_{400} = T_p + \int_p^{400} \frac{\partial T}{\partial p}(T_p)\,dp \tag{4}$$

with $\partial T/\partial p(T)$ given by a climatological relationship is computed from the boundary CTD stations. The r.m.s. error in T_{400}, estimated by subsampling CTD casts at the mooring measurement depths and re-computing T_{400} following Eq. (4), is small at 0.07 °C, with associated error in upper layer transport anomaly of 0.3 Sv following Eq. (3). The mooring T_{400} record therefore provides a useful upper layer transport anomaly proxy at the western boundary with an error 1.3 Sv ($\sqrt{(1.3^2 + 0.3^2)}$).

The temperature record at 400 dbar is intermittent (Fig. 9(I)) during the period of the Abaco array from 1986 to 1997 due to some loss of moorings or instruments close to the western boundary. There is a long gap between the end of the Abaco array in late 1997 and the start of the Rapid monitoring in early 2004. Using Eq. 3, we define the T_{400} transport anomaly proxy (Fig. 9(II)) whenever there is a temperature record near 400 dbar.

Through the 1980s T_{400} was about 17.5 °C. In 1993, the temperature appears to rise and again in late 1996 temperature at 400 dbar rises to about 17.9 °C. When Rapid monitoring starts in March 2004, the 400 dbar temperature is still high at about 17.9 °C (and it has remained at this level through 2008). There is short term variability in the temperature record; the r.m.s. temperature variation is 0.32 °C and hence the associated T_{400} transport variability is 4 Sv, but the time series can be averaged in

time (6-month running mean is shown in Fig. 9) to filter out the short-term variability that masks any trend in the hydrographic end station analysis. Thus, for the mooring time series the smoothed 400 dbar temperature is almost 0.4 °C warmer in 2004/2005 than in the late 1980s. Such temperature change is well above the 0.07 °C uncertainty in 400 dbar temperature due to uncertainties in adjusting for mooring motion. If the eastern boundary conditions were constant over this time, the western boundary warming implies an increase in the overall mid-ocean thermocline slope and accordingly, basin-wide southward transport of the 0–800 m layer. This is seen in the 2 Sv negative transport anomaly of the temperature transport proxy after 1996 (Fig. 9(II)).

Unfortunately no suitable moored time series of temperature and pressure observations are available within the eastern boundary study region. While moorings were deployed around the Canary Islands as part of projects such as ESTOC and CANIGO, they are unsuitable due to intervening topography between them and the eastern boundary of the 26°N section. The only other mooring with long term deployments in the eastern basin of the subtropical north Atlantic is Kiel-276, maintained since 1980 (e.g. Siedler et al., 2005). At a nominal location of 33°N, 22°W, this mooring is close to the Azores Front and inference of changes in the subtropical gyre recirculation is therefore complicated by frontal meanders (Longworth, 2007) and is not pursued here. Thus, we were unable to locate suitable moored time series measurements near the eastern boundary for the period 1980–2005 with which to analyse variations in layer transport anomalies in a similar manner to the western boundary moorings.

From the available mooring time series, the thermocline temperature at the western boundary is significantly warmer by 0.4 °C at 400 dbar in 2005 than it was in the 1980s. This warming suggests that there has been an increase in southward thermocline transport of about 2 Sv from the 1980s to 2005. Although we found that any interannual variability estimated from western boundary hydrographic end station layer transport anomalies is insignificant, here the 400 dbar warming is a statistically significant result and corresponds dynamically to an increase in southward thermocline transport of 2 Sv between the 1980s and 2005. Combined with the significant freshening of deep waters near the
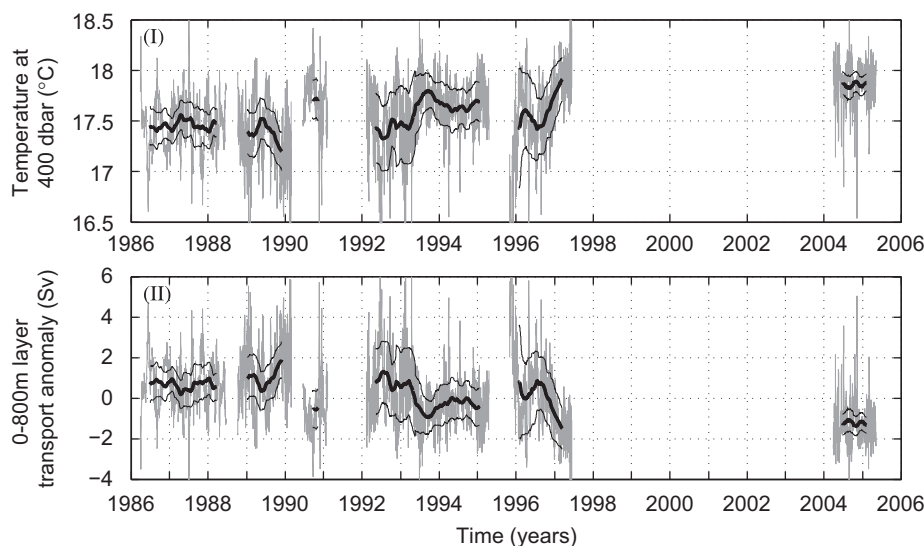
Fig. 9. (I) Temperature at 400 dbar and (II) upper layer T_{400} transport anomaly proxy at 12 h resolution in grey and overlaid by 6-month running mean (heavy black). 95% confidence limits (thin black) are ± 2 standard errors, equal to $\sqrt{((6\ month\ variance)/N^*)}$ where N^* is the number of independent samples in the yearly mean using integral timescales of the T_{400} time series (Longworth, 2007) ranging from 11 to 44 days.

western boundary that is dynamically associated with a decrease in southward deep water transport of 4 Sv, this thermocline warming suggests a reduction in the overturning circulation from the 1980s to 2005 of 2–4 Sv.

4. Discussion

The calculated trends in layer transports at the western boundary suggest a decrease in southward deep water transport of about 3.7 Sv (Table 2) and an increase in southward thermocline transport of 2 Sv (Fig. 9) over 25 years. With the background variability in layer transports of 3–4 Sv and the number of end stations limited to about 40 in the historical database, a trend of 2–3 Sv over 25 years cannot be statistically significant. To detect a statistically significant change of 3 Sv in the presence of the background variability found here, we estimate we would need about 150 independent end stations spread over the 25 years. There were proposals to make fortnightly end stations near the Bahamas and Canary Islands in the early 1980s (Bryden, 1982), and if they had been implemented, we might now be in a position to assess whether a 2–3 Sv change in the overturning has occurred. But our search of the database indicates that such a number of end stations do not exist. Thus, the end station approach to detect statistically significant past changes in the overturning is not likely to be fruitful unless the changes were larger than 6 Sv.

We do find statistically significant changes in the water mass properties at the western boundary, both in the thermocline where the temperature at 400 m depth is 0.4 °C warmer now than in the 1980s and in the deep water where the salinity is 0.008 fresher now than in 1980. In the absence of a detectable trend in the upper layer transport anomaly in the east between 1980 and 2005, the 0.4 °C warming of thermocline waters after 1997 relative to the late 1980s in the western boundary moored 400 dbar temperature time series amounts to a 2 Sv increase in net southward mid-ocean geostrophic transport due to the steeper basin-wide thermocline slope. This is neither supported nor contradicted by the western boundary end station transport anomalies in which unresolved high frequency signals and a method error of comparable size to this transport change prevents detection of any such interannual signal with significance. Taken alone, the 0.008 freshening of DSOW at the western boundary is expected dynamically to be accompanied by a reduction in southward flow of LNADW of approximately 4 Sv between 1980 and 2005. Changes in the UNADW layer are unresolved since these waters include ISOW that has freshened (Fig. 2(I)) and LSW in which properties have fluctuated over the 25 years (e.g. Vaughan and Molinari, 1997). While we calculate a decrease in southward transport of UNADW of 1.3 Sv over 25 years, method errors and lack of resolution of high frequency changes make substantial contributions to the large sub-annual and interannual

variability observed, masking any long term changes that may exist. Therefore while a reduction in southward transport above 800 m of 2 Sv is suggested by the observations, any overall change below 800 m cannot be similarly quantified although the significance and size of the deep freshening do suggest a reduction in southward LNADW transport of 4 Sv between 1980 and 2005.

Because there is some indication that the southward mid-ocean thermocline recirculation has decreased since the 1980s, it is useful to consider the time series of the Florida Straits and Ekman transport over the same period. Neither the annual mean Ekman transport across 26.5°N computed from the NOC monthly mean wind stress climatology (Josey et al., 2002) nor Florida Straits transport from cable measurements (Baringer and Larsen, 2001) shows any long term trend between 1980 and 2005 (Longworth, 2007). The net effect of increased southward transport in the upper 800 m of the mid-ocean section then represents a reduction in the strength of the northward flowing upper limb of the MOC at 26.5°N, or put alternatively an increase in the strength of the mid-ocean thermocline recirculation. A 2 Sv weakening of northward flow in the mid-ocean evident from 1997 onwards compared to the late 1980s is consistent with Wunsch and Heimbach's (2006)'s analysis of a reduction in northward volume flux above 1200 m of 0.19 ± 0.05 Sv yr-1, amounting to 2.3 ± 0.6 Sv over their study period of 1992–2004.

The interpretation of an increase in the mid-ocean recirculation strength over time leads to the question whether or not Sverdrup transport across the section was constant during the study period (e.g. de Boer and Johnson, 2007). Linear regression of Sverdrup transport from the NOC climatology to time shows a 5 Sv increase in southward transport between 1980 and 2004 (Fig. 10). Under such conditions the observed western boundary warming at 400 dbar over time would be interpreted as representative of an increase in the basin-wide thermocline slope associated with increased Sverdrup transport. The NCEP wind stress climatology derived Sverdrup transport, on the other hand, shows a small long term weakening trend with 0.5 Sv less southward transport in 2004 than 1981 (Fig. 10). Following de Boer and Johnson's (2007) argument, this would require any change in the mid-ocean transports above the reference level to occur in the non-linear western boundary regime where mesoscale eddy activity is important. Under this scenario the western boundary warming would be interpreted as decreasing the slope of the thermocline adjacent to the western boundary (where it descends offshore), with a weaker northwards flowing Antilles Current. In the absence of a change in the rest of the mid-ocean section, this still translates to stronger southward transport across the mid-ocean. Thus, regardless of whether or not a long term change in wind stress curl has occurred, the western
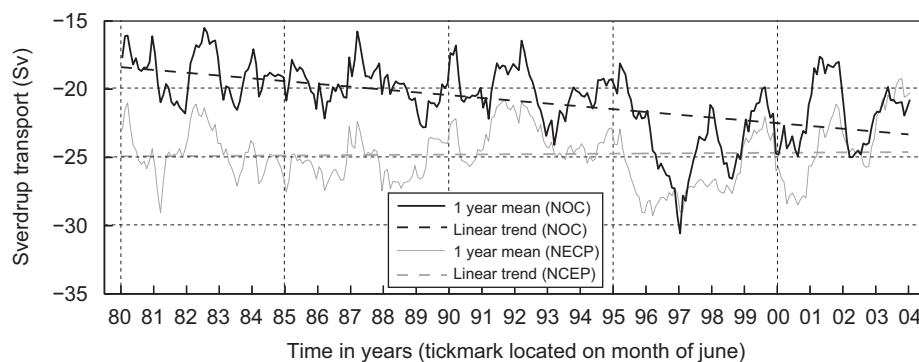

Fig. 10. Sverdrup transport across 25.5°N from the NOC and NCEP monthly wind stress climatologies. Both the 1-year running mean and a linear trend of this to time are plotted. (from Louise Duncan, personal communication).

boundary warming does represent strengthened southward transport of thermocline waters over the past 25 years.

5. Conclusions

Analysis of end-point measurements near 26.5°N based on historical hydrography and moored time series has expanded the estimates of changes in the strength of the MOC over the simple 5 points used by Bryden et al. (2005) and has shown the range of variability in eastern and western boundary stations. End station layer transport anomalies from historical CTD stations remain limited by temporally sparse sampling and are therefore affected by unresolved high frequency signals and are sensitive to location errors of a few Sverdrups. These effects combine to prevent detection of any significant long term trends in mid-ocean geostrophic transport over the 25 years from the CTD end stations and emphasise the importance of continuous monitoring for the future.

In this analysis of end station observations, two significant changes are identified. First, moored temperature records provide evidence for warming in the thermocline at the western boundary since the 1980s, which signifies either increased southward recirculation in the mid-ocean thermocline or reduced northward Antilles Current transport; clarification of this issue is partially dependent on the resolution of discrepancies between trends in wind stress curl of the NOC and NCEP wind stress climatologies. In either case this boundary warming in the thermocline acts to increase the net southward transport above 800 m across the mid-ocean section, consistent in sign with, but weaker than, the 1998 and 2004 hydrographic section transport changes relative to the 1981/1992 baseline state reported by Bryden et al. (2005). Secondly, there is evidence for a significant freshening of the deep waters near the western boundary with LNADW becoming 0.008 fresher over 25 years. Such boundary freshening decreases the net southward deep water transport across the mid-ocean section, consistent with a weakening MOC. Together, on interannual timescales, the baroclinic transport anomalies associated with upper warming and deep freshening at the western boundary suggest a reduction in strength of the Atlantic MOC at 26.5°N between 1980 and 2005 of 2–4 Sv. Such a reduction in MOC transport, however, cannot be statistically validated from the available CTD end stations due to the inherent variability in layer transports of the order 4 Sv and to the limited number of end stations in the historical database.

Acknowledgments

Appendix 1

See (Table A1).

Appendix 2

See (Tables A2.1 and A2.2).

Appendix 3

See (Table A3).

Table A1

Selected eastern boundary end stations. Day is the date of the month, Origin is data source; S—transatlantic hydrographic section, W—World Ocean Database 2001, M-NOC mooring cruise, K-IFM Kiel, H-Hydrobase 2003, Dist. is distance from 800 m isobath, Depth is the station depth and dSal the salinity calibration offset applied (see text).

	Aug.-81	Jul.-83	Nov.-84	Nov.-87	Jun.-88	Aug.-88	Oct.-91	Jun.-92	Jul.-92	Dec.-92	Sep.-94	Jan.-98	Apr.-98	Jul.-03	May-04	Apr.-05
Upper layer																
Day	12th		11th				22nd	12th	21st	9th	30th	24th			9th	5th
Origin	S		W				W	W	S	W	K	S			S	M
Lon. (°E)	−13.55		−16.77				−14.42	−17.10	−16.93	−17.57	−14.81	−13.55			−13.55	−16.15
Lat. (°N)	27.85		25.38				27.50	23.94	24.50	24.39	27.54	27.85			27.85	26.92
Dist (km)	6		45				68	12	32	79	98	6			6	111
Depth (m)	972		2793				1001	981	1403	1929	2498	1070			1081	3483
dSal																0.0044
Middle layer																
Day	13th		11th	15th	4th				22nd			25th	28th		8th	5th
Origin	S		W	W	W				S			S	H		S	M
Lon. (°E)	−15.58		−17.06	−20.00	−21.05				−19.58			−16.11	−21.34		−15.59	−16.15
Lat. (°N)	−27.23		25.51	25.00	24.70				24.51			27.03	24.00		27.23	26.92
Dist. (km)	117		76	332	409				261			119	424		118	111
Depth (m)	3095		3204	3927	4298				3323			3470	4426		3131	3483
dSal	0.0066		0.0027	0.0057	0.0015				0.0055			0.0058	0.001		0.0054	0.0044
Deep layer																
Day	15th	28th				14th			25th			28th		18th	5th	
Origin	S	W				W			S			S		H	S	
Lon. (°E)	−24.29	−24.00				−25.83			−24.67			−24.22		−25.06	−23.50	
Lat. (°N)	24.47	24.00				26.04			24.50			24.50		27.00	24.51	
Dist. (km)	727	690				912			765			720		876	648	
Depth (m)	5114	5056				5269			5110			5124		5230	5003	
dSal	−0.0003	0.0007				0.0040			−0.0004			0.0015		0.0008	0.0011	

Table A2.1

Selected western boundary upper, intermediate and middle layer end stations. Source is the data source; sectn—transatlantic hydrographic section, wod01—World Ocean Database 2001, aomlw—NOAA/AOML and hybas—Hydrobase 2003. Dist. is the distance from the 800 m isobath, Depth is station depth and dSal the salinity calibration offset applied.

Intermediate/middle layer (800–1100 m and 1100–3000 m)							Upper layer (0–800 m)						
Date	Source	Dist. (km)	Depth (m)	Lat. (°N)	Lon. (°E)	dSal	Date	Source	Dist. (km)	Depth (m)	Lat .(°N)	Lon. (°E)	dSal
4-Sep.-81	sectn	6	3483	24.49	−75.42	−0.0019	4-Sep.-81	sectn	4	2837	24.47	−75.44	−0.0001
3-Nov.-81	wod01	8	3624	26.56	−76.77	0.0023	25-Apr.-85	wod01	6	1092	26.72	−76.95	NaN
25-Apr.-85	wod01	7	3468	26.55	−76.78	0.0012	11-May-85	wod01	8	3624	26.56	−76.77	0.0023
11-May-85	wod01	11	3507	26.53	−76.75	0.0005	29-Aug.-85	wod01	7	3468	26.55	−76.78	0.0012
29-Aug.-85	wod01	12	3529	26.55	−76.73	0.0024	19-Jan.-86	wod01	1	1027	26.55	−76.84	NaN
19-Jan.-86	wod01	10	3460	26.55	−76.75	0.0016	5-Feb.-86	wod01	12	3529	26.55	−76.73	0.0024
5-Feb.-86	wod01	12	3603	26.53	−76.74	0.0004	23-Jul.-86	wod01	10	3460	26.55	−76.75	0.0016
22-Jul.-86	wod01	12	3744	26.51	−76.73	0.0015	18-Nov.-86	wod01	1	1080	26.54	−76.84	NaN
18-Nov.-86	wod01	9	3552	26.54	−76.76	0.0015	19-Mar.-87	wod01	12	3744	26.51	−76.73	0.0015
19-Mar.-87	wod01	10	3581	26.55	−76.75	0.0011	27-Mar.-87	wod01	3	1481	26.59	−76.84	NaN
27-Mar.-87	wod01	8	3617	26.55	−76.77	−0.0016	3-Sep.-87	wod01	1	1339	26.56	−76.85	NaN
3-Sep.-87	wod01	12	3198	26.53	−76.73	−0.0008	7-Oct.-88	wod01	2	1268	26.56	−76.85	NaN
8-Oct.-88	wod01	10	3597	26.55	−76.75	−0.0006	13-Mar.-89	wod01	1	1055	26.54	−76.85	NaN
13-Mar.-89	aomlw	11	3061	26.55	−76.75	0.0001	28-Feb.-90	wod01	1	1148	26.54	−76.84	NaN
28-Feb.-90	hybas	19	4527	26.50	−76.67	−0.0002	20-Jun.-90	aomlw	2	1343	26.57	−76.85	NaN
18-Jun.-90	hybas	14	4817	24.25	−74.33	0.0007	27-Jun.-90	hybas	7	1412	26.49	−76.82	NaN
28-Jun.-90	hybas	14	4522	25.51	−76.35	0.0014	29-Jun.-90	hybas	2	2277	24.26	−74.45	NaN
29-Jun.-90	hybas	10	3876	26.51	−76.76	0.0004	9-Jan.-91	hybas	14	4522	25.51	−76.35	0.0014
30-Jun.-90	hybas	9	3544	26.53	−76.76	0.0042	15-Jun.-91	hybas	13	1414	26.49	−76.74	NaN
9-Jan.-91	hybas	10	3554	26.52	−76.76	0.0009	22-Sep.-91	hybas	10	3876	26.51	−76.76	0.0004
15-Jun.-91	hybas	7	3323	24.55	−75.46	−0.0014	20-Jul.-92	hybas	9	3544	26.53	−76.76	0.0042
22-Sep.-91	hybas	4	3014	24.00	−74.36	−0.0026	5-Aug.-92	hybas	10	3554	26.52	−76.76	0.0009
20-Jul.-92	hybas	14	3843	26.50	−76.72	−0.0034	11-Aug.-92	hybas	7	3323	24.55	−75.46	−0.0014
4-Aug.-92	sectn	7	3321	24.55	−75.46	−0.0016	14-Aug.-92	hybas	2	1335	24.00	−74.40	NaN
11-Aug.-92	aomlw	17	4334	26.50	−76.68	0.0014	2-Jun.-93	hybas	2	1399	26.54	−76.83	NaN
14-Aug.-92	aomlw	18	4428	26.50	−76.68	0.0007	13-Jul.-94	sectn	7	3321	24.55	−75.46	−0.0016
30-Mar.-94	aomlw	17	4583	26.50	−76.69	0.0031	8-Mar.-96	aomlw	6	1017	26.50	−76.85	NaN
10-Jul.-96	hybas	11	3869	26.50	−76.75	0.0002	10-Jul.-96	hybas	4	1282	26.52	−76.83	NaN
31-Jul.-96	aomlw	11	3869	26.50	−76.75	0.0005	31-Jul.-96	aomlw	4	1280	26.52	−76.83	NaN
11-Jun.-97	hybas	10	3871	26.51	−76.75	−0.0005	11-Jun.-97	hybas	10	3871	26.51	−76.75	−0.0005
22-Feb.-98	sectn	11	3849	26.50	−76.75	0.0003	22-Feb.-98	sectn	6	1370	26.50	−76.82	NaN
28-Apr.-01	aomlw	13	3842	26.50	−76.73	−0.0018	28-Apr.-01	aomlw	13	3842	26.50	−76.73	−0.0018
26-Jun.-02	aomlw	11	3759	26.50	−76.76	0.0013	26-Jun.-02	aomlw	4	1075	26.52	−76.83	NaN
11-Feb.-03	aomlw	14	3916	26.50	−76.72	−0.0042	11-Feb.-03	aomlw	4	1083	26.52	−76.84	NaN
7-Apr.-04	sectn	11	3815	26.52	−76.75	−0.0002	8-Apr.-04	sectn	5	1709	26.53	−76.81	NaN
2-Oct.-04	aomlw	10	3551	26.50	−76.77	0.0019	2-Oct.-04	aomlw	10	3551	26.50	−76.77	0.0019
8-May-05	aomlw	10	3793	26.50	−76.76	−0.0020	8-May-05	aomlw	4	1083	26.52	−76.83	NaN
23-May-05	aomlw	11	3856	26.50	−76.76	−0.0003	23-May-05	aomlw	4	1036	26.52	−76.84	NaN
21-Sep.-05	aomlw	10	3485	26.50	−76.77	0.0002	20-Sep.-05	aomlw	3	1092	26.52	−76.83	NaN

Table A2.2

Selected western boundary deep layer end stations. Source is the data source; sectn—transatlantic hydrographic section, wod01—World Ocean Database 2001, aomlw—NOAA/AOML and hybas—Hydrobase 2003. Dist. is distance from the 800 m isobath, Depth is station depth and dSal the salinity calibration offset applied. The duplicate columns for variables refer to the shallower (prefix M) and deeper (prefix L) CTD casts, which are appended down the slope.

Deep layer (3000–4700 m)											
M. Date	L. Date	Source	M. Depth (m)	L. Depth (m)	M. Lat (°N)	L. Lat (°N)	M. Lon (°E)	L. Lon (°E)	L. dist (km)	Separation (km)	M. dSal
4-Sep.-81	3-Sep.-81	sectn	3483	4826	24.49	24.50	−75.42	−74.41	27	21	−0.0019
5-Feb.-86	6-Feb.-86	wod01	3460	4799	26.55	26.54	−76.75	−76.52	33	23	0.0016
23-Jul.-86	22-Jul.-86	wod01	3603	4719	26.53	26.54	−76.74	−76.53	32	21	0.0004
18-Nov.-86	19-Nov.-86	wod01	3744	4741	26.51	26.54	−76.73	−76.52	33	20	0.0015
19-Mar.-87	19-Mar.-87	wod01	3552	4791	26.54	26.53	−76.76	−76.54	31	22	0.0015
27-Mar.-87	28-Mar.-87	wod01	3581	4725	26.55	26.54	−76.75	−76.53	32	23	0.0011
3-Sep.-87	3-Sep.-87	wod01	3617	4813	26.55	26.55	−76.77	−76.54	31	23	−0.0016
13-Mar.-89	14-Mar.-89	wod01	3597	4712	26.55	26.54	−76.75	−76.54	30	20	−0.0006
28-Feb.-90	28-Feb.-90	aomlw	3061	4815	26.55	26.54	−76.75	−76.53	32	22	0.0001
20-Jun.-90	20-Jun.-90	hybas	4527	4813	26.50	26.52	−76.67	−76.53	33	14	−0.0002
27-Jun.-90	27-Jun.-90	hybas	4817	4817	24.25	24.25	−74.33	−74.33	14	0	0.0007
29-Jun.-90	29-Jun.-90	hybas	4522	4798	25.51	25.49	−76.35	−76.19	19	5	0.0014
9-Jan.-91	10-Jan.-91	hybas	3876	4821	26.51	26.47	−76.76	−76.53	33	23	0.0004
20-Jul.-92	20-Jul.-92	hybas	3323	4715	24.55	24.62	−75.46	−75.32	24	17	−0.0014
5-Aug.-92	5-Aug.-92	hybas	3014	4748	24.00	24.01	−74.36	−74.28	12	8	−0.0026
11-Aug.-92	10-Aug.-92	hybas	3843	4777	26.50	26.46	−76.72	−76.61	25	12	−0.0034
14-Aug.-92	14-Aug.-92	sectn	3321	4713	24.55	24.61	−75.46	−75.30	24	17	−0.0016
8-Mar.-96	8-Mar.-96	aomlw	4583	4832	26.50	26.50	−76.69	−76.51	35	17	0.0031
10-Jul.-96	10-Jul.-96	hybas	3869	4836	26.50	26.43	−76.75	−76.52	36	25	0.0002

Table A2.2 (continued)

Deep layer (3000–4700 m)

M. Date	L. Date	Source	M. Depth (m)	L. Depth (m)	M. Lat (°N)	L. Lat (°N)	M. Lon (°E)	L. Lon (°E)	L. dist (km)	Separation (km)	M. dSal
31-Jul-96	30-Jul.-96	aomlw	3869	4836	26.50	26.43	−76.75	−76.52	36	25	0.0005
22-Feb.-98	21-Feb.-98	sectn	3849	4720	26.50	26.50	−76.75	−76.62	24	13	0.0003
28-Apr.-01	28-Apr.-01	aomlw	3842	4708	26.50	26.50	−76.73	−76.61	24	11	−0.0018
26-Jun.-02	25-Jun.-02	aomlw	3759	4734	26.50	26.50	−76.76	−76.61	24	13	0.0013
11-Feb-03	11-Feb.-03	aomlw	3916	4812	26.50	26.50	−76.72	−76.60	26	11	−0.0042
8-Apr.-04	9-Apr.-04	sectn	3815	4820	26.52	26.50	−76.75	−76.53	33	22	−0.0002
2-Oct.-04	1-Oct.-04	aomlw	3551	4810	26.50	26.50	−76.77	−76.57	29	19	0.0019
8-May-05	8-May-05	aomlw	3793	4808	26.50	26.50	−76.76	−76.57	28	18	−0.0020
23-May-05	22-May-05	aomlw	3856	4802	26.50	26.50	−76.76	−76.57	28	18	−0.0003
20-Sep.-05	19-Sep.-05	aomlw	3485	4797	26.50	26.50	−76.77	−76.76	10	1	0.0002

Table A3

Abaco and RAPID array western boundary data availability. Nominal instrument depths are for temperature sensors and also pressure if *. If no useable data was recovered from a given instrument it is not listed, e.g. wb1's 50 and 100 m temperature records are bad and therefore omitted from the table. Similarly for the RAPID moorings, all levels had pressure sensors but they are not recorded here if the data is bad. Positions A, wb1 and A_1, are 5, 6 and 9 km from the 800 m isobath.

Array	Mooring	Position	Start date	End date	Water depth (m)	Nominal instrument depths (m)					
Stacs-7	224	A1	28-Mar.-86	27-Mar.-87	3593	150*	400*	1150*	2593	3093	3493
Stacs-8	230	A1	30-Mar.-87	20-Jun.-88	3593	100*	400*	1200	2200	3100	3500
Stacs-10	250	A	9-Oct.-88	23-Apr.-90	900	100*	400	800			
WATTS	268	A	19-Jun.-90	1-Jan.-92	900	100	400*	800*			
ACCP-1	296	A	11-Feb.-92	2-Oct.-93	824	70*	370*	770			
ACCP-2	310	A	29-Sep.-93	24-Dec.-95	856	50	350*	650			
ACCP-3	329	A	31-Oct.-95	12-Jun.-97	1006	100*	400*	700			
Rapid	wb1_1	wb1	27-Mar.-04	9-May-05	1382	250*	400	600*	800*	1000*	
						1200*	1375*	1382*			

References

Arhan, M., Colin de Verdiere, A., Mémery, L., 1994. The eastern boundary of the subtropical North Atlantic. Journal of Physical Oceanography 24, 1295–1316.

Baringer, M.O.N., Larsen, J.C., 2001. Sixteen years of Florida Current transport at 27°N. Geophysical Research Letters 28, 3179–3182.

Baringer, M.O., Molinari, R., 1999. Atlantic Ocean baroclinic heat flux at 24 and 26°N. Geophysical Research Letters 26, 353–356.

Berry, D.I., Kent, E.C., 2009. A new air–sea interaction gridded dataset from ICOADS with uncertainty estimates. Bulletin of the American Meteorological Society 90, 645–656.

de Boer, A.M., Johnson, H.L., 2007. Inferring the zonal distribution of measured changes in the meridional overturning circulation. Ocean Science 3, 55–57.

Bryden, H.L., 1982. Ocean heat transport. Papers Presented at the Meeting on Time Series of Ocean Measurements (Tokyo, 11–15 May 1981). World Climate Programme Report WCP-21, pp. 3–12.

Bryden, H.L., Longworth, H.R., Cunningham, S., 2005. Slowing of the Atlantic Meridional Overturning Circulation at 25°N. Nature 438, 655–657.

Bryden, H.L., Griffiths, M.J., Lavín, A., Millard, R.C., Parrilla, G., Smethie, W.M.J., 1996. Decadal changes in water mass characteristics at 24°N in the subtropical North Atlantic Ocean. Journal of Climate 12, 3162–3186.

Cubasch, U., Meehl, G.A., Boer, G.J., Stouffer, R.J., Dix, M., Noda, A., Senior, C.A., Raper, S., Yap, K.S., 2001. Projections of future climate change. Climate change 2001: the scientific basis. In: Houghton, J.T., Ding, Y., Griggs, D.J., Noguer, M., Linden, P.J.V.D., Dai, X., Maskell, K., Johnson, C.A. (Eds.), Contribution of Working Group I to the Third Assessment Report of the Intergovernmental Panel on Climate Change. Cambridge University Press, pp. 525–582.

Cunningham, S.A., Kanzow, T., Rayner, D., Baringer, M.O., Johns, W.E., Marotzke, J., Longworth, H.R., Grant, E.M., Hirschi, J.-J.M., Beal, L.M., Meinen, C.S., Bryden, H.L., 2007. Temporal variability of the Atlantic Meridional Overturning Circulation at 26.5°N. Science 317, 935–938.

Curry, R.G., McCartney, M.S., 2001. Ocean gyre circulation changes associated with the North Atlantic Oscillation. Journal of Physical Oceanography 31, 3374–3400.

Dickson, B., Yashayaev, I., Meincke, J., Turrell, B., Dye, S., Holfort, J., 2002. Rapid freshening of the deep North Atlantic Ocean over the past four decades. Nature 416, 832–837.

Fine, R.M., 1995. Tracers, time scales, and the thermohaline circulation: the lower limb in the North Atlantic Ocean. Reviews of Geophysics 33, 1353–1365.

Fine, R.M., Molinari, R., 1988. A continuous deep western boundary current between Abaco (26.5°N) and Barbados (13°N). Deep-Sea Research 35, 1441–1450.

Ganachaud, A., 2003. Error budget of inverse box models: the North Atlantic. Journal of Atmospheric and Oceanic Technology 20, 1641–1655.

Hall, M.M., Bryden, H.L., 1982. Direct estimates and mechanisms of ocean heat transport. Deep-Sea Research 29, 339–359.

Hirschi, J., Baehr, J., Marotzke, J., Stark, J., Cunningham, S., Beismann, J.-O., 2003. A monitoring design for the Atlantic Meridional Overturning Circulation. Geophysical Research Letters 30 (7), 1413. doi:10.1029/2003GL016776.

Johns, W.E., Kanzow, T., Zantopp, R.J., 2005. Estimating ocean transports with dynamic height moorings: an application in the Atlantic Deep Western Boundary Current at 26°N. Deep-Sea Research I 52, 1542–1567.

Josey, S.A., Kent, E.C., Taylor, P.K., 2002. Wind stress forcing of the ocean in the SOC climatology: comparisons with the NCEP-NCAR, ECMWF, UWM/COADS, and Hellerman and Rosenstein Datasets. Journal of Physical Oceanography 32, 1994–2019.

Kanzow, T., Cunningham, S.A., Rayner, D., Hirschi, J.J-M., Johns, W.E., Baringer, M.O., Bryden, H.L., Beal, L.M., Meinen, C.S., Marotzke, J., 2007. Observed flow compensation associated with the MOC at 26.5°N in the Atlantic. Science 317, 938–941.

Lavín, A., Bryden, H.L., Parrilla, G., 1998. Meridional transport and heat flux variations in the subtopical North Atlantic. The Global Atmosphere and Ocean System 6, 269–293.

Lavín, A.M., Bryden, H.l., Parrilla, G., 2003. Mechanisms of heat, freshwater, oxygen and nutrient transports and budgets at 24.5°N in the subtropical North Atlantic. Deep-Sea Research I 50, 1099–1128.

Leaman, K.D., Harris, J.E., 1990. On the average absolute transport of the deep western boundary currents east of Abaco Island, the Bahamas. Journal of Physical Oceanography 20, 467–475.

Lee, T.N., Johns, W.E., Zantopp, R.J., Fillenbaum, E.R., 1996. Moored observations of Western Boundary Current variability and Thermohaline Circulation at 26.5°N in the subtropical North Atlantic. Journal of Physical Oceanography 26, 962–983.

Longworth, H. R., 2007. Constraining variability of the Atlantic Meridional Overturning Circulation at 25°N from historical observations. Ph.D. Thesis, School of Ocean and Earth Science, University of Southampton. Southampton, United Kingdom, 200p.

Lynch-Stieglitz, J., 2001. Using ocean margin density to constrain ocean circulation and surface wind strength in the past. Geochemistry, Geophysics, Geosystems, 2, Paper number 2001GC000208.

Mantyla, A.W., 1994. The treatment of inconsistencies in Atlantic deep water salinity data. Deep-Sea Research I 41, 1387–1405.

Marotzke, J., Giering, R., Zhang, K.Q., Stammer, D., Hill, C., Lee, T., 1999. Construction of the adjoint MIT ocean general circulation model and application to

Atlantic heat transport sensitivity. Journal of Geophysical Research 104 (C12), 29529–29547.

Mittelstaedt, E., 1991. The ocean boundary along the northwest African Coast: circulation and oceanographic properties at the sea surface. Progress in Oceanography 26, 307–355.

Molinari, R.L., Johns, E., Festa, J., 1990. The annual cycle of meridional heat flux in the Atlantic Ocean at 26.5°N. Journal of Physical Oceanography 20, 476–482.

Molinari, R.L., Fine, R.A., Wilson, W.D., Curry, R.G., Abell, J., McCartney, M.S., 1998. The arrival of recently formed Labrador Sea Water in the Deep Western Boundary Current at 26.5°N. Geophysical Research Letters 25, 2249–2252.

Müller, T., Siedler, G., 1992. Multi-year current time series in the eastern North Atlantic Ocean. Journal of Marine Research 50, 63–98.

Olson, D.B., Schott, F.A., Zantopp, R.J., Leaman, K.D., 1984. The mean circulation east of the Bahamas as determined from a recent measurement program and historical XBT data. Journal of Physical Oceanography 14, 1470–1487.

Pond, S., Pickard, G.L., 1983. Introductory Dynamical Oceanography 2nd Edition Butterworth-Heinemann 329pp.

Roemmich, D., Wunsch, C., 1985. Two transatlantic sections: meridional circulation and heat flux in the subtropical North Atlantic Ocean. Deep-Sea Research 32, 619–664.

Sato, O., Rossby, T., 1995. Seasonal and low frequency variations in dynamic height anomaly and transport of the Gulf Stream. Deep-Sea Research 42, 149–164.

Saunders, P.M., 1986. The accuracy of measurements of salinity oxygen, and temperature in the deep ocean. Journal of Physical Oceanography 16, 189–195.

Saunders, P., 1987. Flow through discovery gap. Journal of Physical Oceanography 17, 631–643.

Siedler, G., Armi, L., Müller, T., 2005. Meddies and decadal changes at the Azores Front from 1980 to 2000. Deep-Sea Research II 52, 583–604.

Stouffer, R.J., Yin, J., Gregory, J.M., Dixon, K.W., Spelman, M.J., Hurlin, W., Weaver, A.J., Eby, M., Flato, G.M., Hasumi, H., Hu, A., Jungclaus, J.H., Kamenkovich, I.V., Levermann, A., Montoya, M., Murakami, S., Nawrath, S., Oka, A., Peltier, W.R., Robitaille, D.Y., Sokolov, A., Vettoretti, G., Weber, S.L., 2006. Investigating the causes of the response of the thermohaline circulation to past and future climate changes. Journal of Climate 19 (8), 1365–1387.

Vaughan, S.L., Molinari, R.L., 1997. Temperature and salinity variability in the Deep Western Boundary Current. Journal of Physical Oceanography 27, 749–761.

Wunsch, C., Heimbach, P., 2006. Estimated decadal changes in the North Atlantic Meridional Overturning Circulation and heat flux 1993–2004. Journal of Physical Oceanography 36, 2012–2024.